

## Three-dimensional electronic structure of superconducting iron pnictides observed by angle-resolved photoemission spectroscopy

Walid MALAEB<sup>1\*</sup>, Teppei YOSHIDA<sup>1,2</sup>, Atsushi FUJIMORI<sup>1</sup>, Masato KUBOTA<sup>3</sup>, Kanta ONO<sup>3</sup>,  
Kunihiro KIHOU<sup>4</sup>, Parasharam M. SHIRAGE<sup>4</sup>,  
Hijiri KITO<sup>4</sup>, Akira IYO<sup>2,4</sup>, Hiroshi EISAKI<sup>2,4</sup>, Yasuyuki NAKAJIMA<sup>2,5</sup>, Tsuyoshi TAMEGAI<sup>2,5</sup>,  
and Ryotaro ARITA<sup>2,5</sup>.

<sup>1</sup>*Department of Complexity Science and Engineering and Department of Physics, University of Tokyo, Bunkyo-ku, Tokyo 113-0033*

<sup>2</sup>*JST, Transformative Research-Project on Iron Pnictides (TRIP), Chiyoda, Tokyo 102-0075*

<sup>3</sup>*Institute for Material Structure Science, High Energy Accelerator Research Organization, Tsukuba, Ibaraki 305-0801*

<sup>4</sup>*National Institute of Advanced Industrial Science and Technology (AIST), Tsukuba, Ibaraki 305-8568*

<sup>5</sup>*Department of Applied Physics, University of Tokyo, Bunkyo-ku, Tokyo 113-8656*

We have performed an angle-resolved photoemission spectroscopy (ARPES) study of the undoped and electron-doped iron pnictides  $\text{BaFe}_{2-x}\text{Co}_x\text{As}_2$  (Ba122) ( $x=0, 0.14$ ) and studied the Fermi surfaces (FSs) and band dispersions near the Fermi level. The FS sheets we observed are consistent with the shrinkage of the hole-like pockets around the Brillouin Zone (BZ) center and the expansion of the electron pockets around the BZ corner in the electron-doped compound as compared to the undoped parent compound. Band dispersions and FSs around the BZ center strongly depend on the photon energy, indicating the three-dimensional (3D) electronic structure. This observation suggests that the antiferromagnetism and superconductivity in the pnictides may have to be considered including the orbital-dependent 3D electronic structure, where FS nesting is not necessarily strong.

KEYWORDS: pnictides, three-dimensional electronic structure, ARPES

The discovery of superconductivity (SC) in layered iron pnictides<sup>1</sup> with the critical temperature  $T_c$  reaching  $\sim 56$  K<sup>2</sup> has opened a new route for the high- $T_c$  research in addition to that of the cuprates, bringing new challenges to the materials science community on both experimental and theoretical sides. This new class of iron-based systems share some common properties with the cuprates such as the layered crystal structures<sup>1</sup> and antiferromagnetic (AFM) ordering in the parent compounds.<sup>3,4</sup> However, many differences exist between the two families especially in their electronic structures. These differences started to appear from the early stage when local-density-approximation (LDA) band-structure calculations predicted that all the Fe  $3d$ -derived bands exist near the Fermi level ( $E_F$ ), resulting in complicated hole- and electron-like Fermi surface (FS) sheets,<sup>5-7</sup> whereas only a single band with one FS (hole- or

---

\*malaeb@wyvern.phys.s.u-tokyo.ac.jp

electron- like) exists in the cuprates. The predictions of the LDA calculations were confirmed by photoemission experiments, which demonstrated that Fe  $3d$  states are predominant near  $E_F$ <sup>8-10</sup> with moderate  $p-d$  hybridization and electron correlation.<sup>9</sup> More detailed features of the electronic structure came from angle-resolved photoemission spectroscopy (ARPES): (i) Several disconnected hole-like and electron-like FS sheets,<sup>11</sup> (ii) kinks in the dispersions, suggesting coupling of quasiparticles to Boson excitations,<sup>12,13</sup> (iii) moderately renormalized energy bands due to electron correlation,<sup>14,15</sup> and (iv) FS-dependent nodeless, nearly-isotropic superconducting gaps.<sup>16-19</sup> Most of these results give reasonable agreement with the band-structure calculations. Nevertheless, many other features of the electronic structure, predicted by the calculations and necessary for understanding the occurrence of SC in the iron pnictides, have not been observed yet by ARPES.

Among these features is the three-dimensional (3D) electronic structure of  $A\text{Fe}_2\text{As}_2$  ( $A$ =Alkaline earth) (122 family) and its doped compounds predicted by band-structure calculations<sup>20-22</sup> as compared to the quasi-two-dimensional electronic structure of the cuprates. Such a three-dimensionality has been supported by recent experimental reports such as the weak anisotropy of the upper critical field  $H_{c2}$  in  $(\text{Ba,K})\text{Fe}_2\text{As}_2$ <sup>23</sup> and  $\text{Ba}(\text{Fe,Co})_2\text{As}_2$ <sup>24,25</sup> (Ba122). The weak anisotropy of  $H_{c2}$  was attributed to the 3D FSs in these compounds. Here, we show a direct observation of the 3D electronic structure in iron pnictides by ARPES. Our results on the AFM parent compound  $\text{BaFe}_2\text{As}_2$  and the superconducting compound  $\text{BaFe}_{1.86}\text{Co}_{0.14}\text{As}_2$  show that the FS in the Brillouin Zone (BZ) center ( $\Gamma$  point) has strong modulation along the  $k_z$  direction, whereas the FS at the BZ corner (X point) is almost cylinder-like with weak  $k_z$  modulation especially in the undoped sample. This is in good agreement with the band-structure calculations<sup>20-22</sup> and the  $H_{c2}$  measurements.<sup>23-25</sup> The three-dimensionality of the FS around the  $\Gamma$  point was reported by two recent ARPES studies,<sup>26,27</sup> consistent with the present results. However, in Ref. [27] the three-dimensionality was reported to exist only in the AFM state below the structural/magnetic transition temperature ( $T_S$ ) of the undoped compound. Our results show that the superconducting  $\text{Ba}(\text{Fe,Co})_2\text{As}_2$  sample has similarly strong three dimensionality, yielding important implications for the mechanism of SC as well as for the origin of the antiferromagnetism.

High-quality single crystals of the parent compound  $\text{BaFe}_2\text{As}_2$  and the electron-doped compound  $\text{BaFe}_{1.86}\text{Co}_{0.14}\text{As}_2$  ( $T_c=24$  K) were grown using the flux method.<sup>28</sup> ARPES measurements were carried out at BL-28A of Photon Factory (PF) using a circularly-polarized light with photon energies ranging between 35 and 90 eV. A Scienta SES-2002 analyzer was used with the total energy resolution of  $\sim 20$  meV and the momentum resolution of  $\sim 0.02\pi/a$ , where  $a=3.9\text{\AA}$  is the in-plane lattice constant. The crystals were cleaved *in situ* at  $T=10$  K in an ultra-high vacuum below  $1\times 10^{-10}$  Torr giving flat mirror-like surfaces which stayed reasonably stable all over our measuring time ( $\sim 3$  days). Calibration of the  $E_F$  of the samples was achieved by referring to that of gold. We have performed a density functional calculation with the local-density-approximation (LDA) by using the WIEN2k package,<sup>29</sup> where the experimental tetragonal lattice parameters of room temperature  $\text{BaFe}_2\text{As}_2$  were used. As for the internal coordinate of As, Ref. [20] was followed and  $z_{\text{As}}$  was set to be 0.342, which was obtained by LDA total energy minimization.

Figure 1 (a) and (b) show the results of FS mapping at low temperature ( $\sim 10$  K) using photon energy  $h\nu = 60$  eV for the undoped and electron-doped Ba122 compounds, respectively. In these plots, the photoemission intensity has been integrated over 20 meV around  $E_F$ . For both compounds, one can clearly observe a nearly circular-shaped hole pocket centered at the two-dimensional (2D) BZ center (denoted by  $\Gamma$ ) in addition to an electron pocket centered at the 2D BZ corner (denoted by X), in agreement with the previous ARPES results on  $A\text{Fe}_2\text{As}_2$  ( $A$ =Alkaline earth) and their doped compounds.<sup>16,18</sup> The 3D BZ of  $\text{BaFe}_2\text{As}_2$  in the tetragonal phase is shown in Fig. 1 (c) and is used as a reference to indicate high-symmetry points in momentum ( $k$ ) space. Note that the intensity asymmetry observed around  $\Gamma$  and X is due to the photoemission matrix-element effect arising from the circularly-polarized light used in this study. Direct comparison between the two compounds reveals that the hole (electron) pocket becomes smaller (larger) in size with electron doping. Although it shrinks in size, the hole-like FS around  $\Gamma$  does not completely disappear in this case as was observed for more heavily electron-doped  $\text{Ba}(\text{Fe},\text{Co})_2\text{As}_2$ .<sup>30</sup> The features around the X point, which are anisotropic in the undoped compound, are expanded, change their shapes, and become nearly circular with electron doping.

The ARPES intensity plot in energy-momentum ( $E$ - $k$ ) space along cuts 1 (across  $\Gamma$ ) and 2 (across X) for undoped Ba122 taken at  $h\nu = 60$  eV are shown, respectively, in panels (a) and (b) of Fig. 2. In the figure,  $k_{\parallel}$  denotes momenta along cut 1 or cut 2. Panel (a) shows a hole-like band crossing  $E_F$  and giving rise to the hole-like FS around  $\Gamma$  [Fig. 1 (a)]. However, a tiny structure having the features of an electron pocket is observed in this case. This has been interpreted as the result of band folding due to the AFM order also observed in a previous ARPES study of another parent compound of the 122 family,  $\text{SrFe}_2\text{As}_2$ .<sup>31</sup> We note that recent results of quantum oscillation measurements of the parent compound  $\text{BaFe}_2\text{As}_2$  support a conventional band folding picture of the AFM ground state of this compound.<sup>32</sup> As for cut 2 in Fig. 1 (a) (X point), an electron-like band crossing  $E_F$  is observed.

Similar cuts (cuts 1 and 2 in Fig. 1 (b)) were taken for the electron-doped sample  $\text{BaFe}_{1.86}\text{Co}_{0.14}\text{As}_2$  under the same conditions as those of the undoped sample and the corresponding  $E$ - $k$  plots for  $h\nu = 60$  eV are shown in Fig. 3 (a) and (b). Panel (a) shows two hole-like bands (inner and outer) crossing  $E_F$  without signature of the additional electron pocket feature observed for the same cut in the undoped sample [Fig. 2 (a)]. This suggests that electron doping weakens the band folding effects arising from the AFM order. The band leading to the electron-like FS is observed more clearly around X [Fig. 3 (b)]. It should be noted that the dispersions of  $\text{BaFe}_{1.86}\text{Co}_{0.14}\text{As}_2$  in Fig. 3 show some broadening as compared to those of the parent compound  $\text{BaFe}_2\text{As}_2$  (Fig. 2), probably because Co doping increases carrier scattering in the FeAs plane.

Now, we turn to the investigation of possible three-dimensionality in the electronic structure ( $k_z$  dependence) predicted by most of the band-structure calculations on iron pnictides, in particular on 122 compounds.<sup>20-22</sup> These calculations predict different  $k_z$  dependences at different regions in the  $k_x$ - $k_y$  space, namely, a stronger three-dimensionality is expected around the 2D BZ center  $\Gamma$  (or the  $\Gamma$ -Z line in the 3D BZ) rather than the 2D zone corner X (Refer to Fig. 1 (c)). It is well known that by changing the photon

energy in photoemission experiment, one can probe different  $k_z$  values<sup>33</sup> (within the uncertainty of  $k_z \approx 1/\lambda$ , where  $\lambda$  is the photoelectron mean-free path) according to the following formula which relates the wave vector along the  $z$ -direction ( $k_z$ ) to the excitation energy  $h\nu$  for normal emission:

$$k_z = \left[ \frac{2m}{\hbar^2} \right]^{1/2} [(h\nu - \Phi) \cos^2 \theta + V_0]^{1/2}, \quad (1)$$

where  $m$  and  $2\pi\hbar$  are the electron mass and Planck's constant,  $h\nu$  is the photon energy,  $\Phi$  is the work function, and  $V_0$  is the inner potential of the sample.

Thus, we performed a photon-energy dependent ARPES measurement of both samples at two specific regions of  $k$ -space, around the  $\Gamma$  point or around the  $\Gamma$ -Z line (cut 1 in Fig. 1 (a) and (b)) and around the X point (cut 2 in Fig. 1 (a) and (b)). For both samples, the ARPES intensity plots in  $E$ - $k$  space show strong photon-energy dependence along the  $\Gamma$ -Z line. This can be clearly observed by comparing the dispersions in Fig. 2 (a) and (c) for the undoped sample, where the Fermi level crossing occurs at different  $k_F$  values depending on the photon energy ( $h\nu=60$  and  $40$  eV are shown here). This suggests that the corresponding FS centered at the  $\Gamma$  point shows strong photon-energy dependence and consequently strong  $k_z$  dependence as mentioned above. From a large set of photon-energy dependent ARPES data (with photon energies ranging from  $35$  to  $90$  eV) and using Eq. (1), we have constructed the FS images in the  $k_{\parallel}$ - $k_z$  plane containing the  $\Gamma$ -Z line for the undoped sample in Fig. 2 (e). The color scale in this figure represents the photoelectron intensity integrated in a narrow energy window of  $20$  meV around  $E_F$ .  $k_F$  points determined from peak positions in momentum distribution curves (MDCs) are also shown in this plot as black dots. From this plot it becomes clear that the FS shows strong modulation attaining its smallest size around the  $\Gamma$  point [ $\mathbf{k}=(0,0,0)$ ] and its largest size around the Z point [ $\mathbf{k}=(0,0,2\pi/c)$ ]. As for the photon-energy dependence around the X point, Fig. 2 (d) shows the dispersion around the X point for the undoped Ba122 sample (cut 2 in Fig. 1 (a)) at  $h\nu=40$  eV, which when compared with the same data taken at  $h\nu=60$  eV [Fig. 2 (b)] shows only small differences. The FS image in the  $k_{\parallel}$ - $k_z$  plane is constructed as shown in Fig. 2 (f). The image plot shows almost straight cylinders along the  $k_z$  direction and thus weak  $k_z$  dependence, which renders the electronic structure around the BZ corner much less three-dimensional than that observed around the BZ center.

Now we turn to the case of the electron-doped superconducting sample: Fig. 3 (a) and (c) which correspond to cut 1 in Fig. 1 (b), show a clear photon energy dependence of the dispersions as well as  $k_F$  points. The corresponding FS image plot along the  $\Gamma$ -Z line is shown in Fig. 3 (e), where the strong  $k_z$  modulation is quite clear. The dispersions around the X point show weaker photon-energy dependence as can be deduced from those taken at  $h\nu=60$  and  $35$  eV and shown in Fig. 3 (b) and (d), respectively. However, the modulation along  $k_z$  can be clearly seen in the FS image plot in Fig. 3 (f). The three-dimensionality of this FS is stronger than that observed for the undoped sample at the X point [Fig. 2 (f)].

These experimental data are compared with the FSs determined from our LDA band-structure calculations in the paramagnetic state in panels (g) and (h) of Figs. 2 and 3. Because the major effect of AFM

ordering is to fold the energy bands into the AFM BZ and resultant band anticrossing accompanied by intensity redistribution, the global intensity distribution is not dramatically altered by the band folding, which is also confirmed by calculations due to the small magnetic moments in pnictides.<sup>34</sup> We thus find qualitatively good agreement between experiment and calculation although the calculation predicts generally stronger three-dimensionality. We note that the FSs derived from the  $d_{z^2}$  orbitals have stronger  $k_z$  modulation than others. Another discrepancy between experiment and calculation is that the experiment does not necessarily reveal the second FSs (except for some photon energies). In order to observe the second FSs, further experiment with higher statistics and using various photon polarizations will be necessary.

Observing the 3D electronic structure in the parent compound  $\text{BaFe}_2\text{As}_2$ , which shows a collinear AFM spin density wave (SDW),<sup>4</sup> raises the question about the role of FS nesting in driving the AFM state in the parent compounds.<sup>6</sup> Our experimental data and LDA calculations show that the outer hole-like FS sheet around  $\Gamma$  has stronger three-dimensionality as compared to the electron-like FS sheet around X. It seems that the strong three-dimensionality significantly weakens the nesting condition between the two FS sheets, which was proposed to enhance the high- $T_c$  SC in this compound.<sup>16,18,30</sup> Now we discuss the relationship between the three-dimensional electronic structure and SC in iron pnictides. In this class of materials, the 122 family is predicted to have more pronounced three-dimensionality than the 1111 family<sup>35</sup> by the LDA band-structure calculations.<sup>20-22</sup> This may be correlated with the different  $T_c$  values, the highest  $T_c$  ( $\sim 56\text{K}$ ) among the pnictides until now being achieved in the 1111 family<sup>2</sup> as compared to  $\sim 38\text{K}$  in the 122 family.<sup>36</sup> It has also been observed by ARPES that the size of the SC gap is larger in the 1111 family (for example  $\Delta \sim 15$  meV in  $\text{NdFeAsO}_{0.9}\text{F}_{0.1}$ )<sup>17</sup> than in the 122 family (for example  $\Delta \sim 12$  meV in  $\text{Ba}_{0.6}\text{K}_{0.4}\text{Fe}_2\text{As}_2$ <sup>16</sup> and  $\Delta \sim 6.7$  meV in  $\text{BaFe}_{1.85}\text{Co}_{0.15}\text{As}_2$ <sup>18</sup>). Nevertheless, the fairly high- $T_c$  values attained by the 122 family suggest that the high- $T_c$  SC exists not only in systems with low-dimensional electronic structures like cuprates. This is also consistent with the results from  $H_{c2}$  measurements in the 122 system mentioned above.<sup>23-25</sup> According to the LDA band-structure calculations [Fig. 3 (g)], the outer hole-like FS sheet is derived mainly from  $d_{z^2}$  orbitals. In the scenario of spin-fluctuation-mediated SC, the 2D  $x^2 - y^2/xy$  bands play major roles in SC and the  $d_{z^2}$  band is only a "passive" band for SC. The small gap  $\Delta$  for these bands may be regarded as the "passiveness" of the  $d_{z^2}$  band but may not be so "passive" since  $2\Delta/k_B T_c$  is comparable to the active 2D FS in the 1111 compounds. Judging the real contribution of the 3D electronic structure to the SC in iron pnictides needs further investigation.

A recent ARPES report on  $\text{CaFe}_2\text{As}_2$ <sup>27</sup> has shown that its FSs have strong three-dimensionality, consistent with the present study but that a 3D to 2D transition occurs above the orthorhombic-to-tetragonal structural/magnetic transition temperature ( $T_S = 160 \sim 170$  K). While this led the authors to the conclusion that the low dimensionality plays an important role in understanding the superconducting mechanism in pnictides, our results on the superconducting sample  $\text{BaFe}_{1.86}\text{Co}_{0.14}\text{As}_2$  confirm that high- $T_c$  SC exists in pnictides in the three-dimensional electronic structure. Raising the temperature above  $T_S$  and Co-doping in  $\text{AFe}_2\text{As}_2$  destroy the AFM ordering and lead to the orthorhombic-to-tetragonal structural transition. However, this does not necessarily imply that a similar 3D to 2D transition occurs with carrier

doping. As for the case of Co-doping, our ARPES results on superconducting  $\text{BaFe}_{1.86}\text{Co}_{0.14}\text{As}_2$  confirm that the three-dimensionality persists in the SC samples, and that achieving relatively high- $T_c$  SC in iron pnictides with 3D electronic structure is possible although the relationship between three-dimensionality and SC needs further clarification in future studies.

In summary, we have performed an ARPES study on the undoped and electron-doped iron pnictides  $\text{Ba}(\text{Fe},\text{Co})_2\text{As}_2$  and studied the FSs and band dispersions near  $E_F$ . The strong photon-energy dependence of band dispersions and FSs around the BZ center of both the parent and superconducting compounds indicates the 3D electronic structure, where FS nesting should be weakened compared with the 2D electronic structure. These observations suggest that the antiferromagnetism and the AFM ordering and high- $T_c$  SC in the pnictides may have to be considered including the 3D electronic structure.

The authors acknowledge A. Ino, Y. Aiura, Y. Nakashima, Y. Ishida, T. Shimojima and S. Shin for informative discussions and S. Ideta for technical support. This work was supported by a Grant-in-Aid for Scientific Research in Priority Area "Invention of Anomalous Quantum Materials" from the Ministry of Education, Culture, Sports, Science and Technology (MEXT) and by Japan Science and Technology Agency (JST). WM is thankful to MEXT for financial support. Experiment at Photon Factory was approved by the Photon Factory Program Advisory Committee (Proposal No. 2006S2-001).

## References

- 1) Y. Kamihara, T. Watanabe, M. Hirano, and H. Hosono: *J. Am. Chem. Soc.* **130** (2008) 3296.
- 2) C. Wang, L. Li, S. Chi, Z. Zhu, Z. Ren, Y. Li, Y. Wang, X. Lin, Y. Luo, S. Jiang, Z. Xu, G. Cao, and Z. Xu: *Euro Phys. Lett.* **83** (2008) 67006.
- 3) C. de la Cruz, Q. Huang, J. W. Lynn, J. Li, W. Ratcliff II, J. L. Zarestky, H. A. Mook, G. F. Chen, J. L. Luo, N. L. Wang and P. Dai: *Nature* **453** (2008) 899.
- 4) Q. Huang, Y. Qiu, W. Bao, M. A. Green, J. W. Lynn, Y. C. Gasparovic, T. Wu, G. Wu, and X. H. Chen: *Phys. Rev. Lett.* **101** (2008) 257003.
- 5) K. Kuroki, S. Onari, R. Arita, H. Usui, Y. Tanaka, H. Kontani, and H. Aoki: *Phys. Rev. Lett.* **101** (2008) 087004.
- 6) I.I. Mazin, D.J. Singh, M.D. Johannes and M.H. Du: *Phys. Rev. Lett.* **101** (2008) 057003.
- 7) S. Ishibashi, K. Terakura and H. Hosono: *J. Phys. Soc. Jpn.* **77** (2008) 053709.
- 8) T. Sato, S. Souma, K. Nakayama, K. Terashima, K. Sugawara, T. Takahashi, Y. Kamihara, M. Hirano, and H. Hosono: *J. Phys. Soc. Jpn.* **77** (2008) 063708.
- 9) W. Malaeb, T. Yoshida, T. Kataoka, A. Fujimori, M. Kubota, K. Ono, H. Usui, K. Kuroki, R. Arita, H. Aoki, Y. Kamihara, M. Hirano, and H. Hosono: *J. Phys. Soc. Jpn.* **77** (2008) 093714.
- 10) A. Koitzsch, D. Inosov, J. Fink, M. Knupfer, H. Eschrig, S. V. Borisenko, G. Behr, A. Köhler, J. Werner, B. Büchner, R. Follath, and H. A. Dürr: *Phys. Rev. B* **78** (2008) 180506(R).
- 11) C. Liu, T. Kondo, M. E. Tillman, R. Gordon, G. D. Samolyuk, Y. Lee, C. Martin, J. L. McChesney, S. Bud'ko, M. A. Tanatar, E. Rotenberg, P. C. Canfield, R. Prozorov, B. N. Harmon, and A. Kaminski: *Phys. Rev. Lett.* **101** (2008) 177005.
- 12) P. Richard, T. Sato, K. Nakayama, S. Souma, T. Takahashi, Y.-M. Xu, G. F. Chen, J. L. Luo, N. L. Wang and H. Ding: *Phys. Rev. Lett.* **102** (2009) 047003.
- 13) L. Wray, D. Qian, D. Hsieh, Y. Xia, L. Li, J. G. Checkelsky, A. Pasupathy, K. K. Gomes, C. V. Parker, A. V. Fedorov, G. F. Chen, J. L. Luo, A. Yazdani, N. P. Ong, N. L. Wang, and M. Z. Hasan: arXiv: 0812.2061.
- 14) L. X. Yang, Y. Zhang, H. W. Ou, J. F. Zhao, D. W. Shen, B. Zhou, J. Wei, F. Chen, M. Xu, C. He, Y. Chen, Z. D. Wang, X. F. Wang, T. Wu, G. Wu, X. H. Chen, M. Arita, K. Shimada, M. Taniguchi, Z. Y. Lu, T. Xiang, and D. L. Feng: arXiv: 0806.2627.
- 15) D. H. Lu, M. Yi, S.-K. Mo, A. S. Erickson, J. Analytis, J.-H. Chu, D. J. Singh, Z. Hussain, T. H. Geballe, I. R. Fisher, and Z.-X. Shen: *Nature* **455** (2008) 81.
- 16) H. Ding, P. Richard, K. Nakayama, K. Sugawara, T. Arakane, Y. Sekiba, A. Takayama, S. Souma, T. Sato, T. Takahashi, Z. Wang, X. Dai, Z. Fang, G. F. Chen, J. L. Luo, and N. L. Wang: *Euro Phys. Lett.* **83** (2008) 47001.
- 17) T. Kondo, A. F. S.-Syrro, O. Copie, C. Liu, M. E. Tillman, E. D. Mun, J. Schmalian, S. L. Bud'ko, M. A. Tanatar, P. C. Canfield, and A. Kaminski: *Phys. Rev. Lett.* **101** (2008) 147003.
- 18) K. Terashima, Y. Sekiba, J. H. Bowen, K. Nakayama, T. Kawahara, T. Sato, P. Richard, Y.-M. Xu, L. J. Li, G. H. Cao, Z.-A. Xu, H. Ding, and T. Takahashi: arXiv: 0812.3704.
- 19) K. Nakayama, T. Sato, P. Richard, Y.-M. Xu, Y. Sekiba, S. Souma, G. F. Chen, J. L. Luo, N. L. Wang, H. Ding, and T. Takahashi: arXiv: 0812.0663.
- 20) D. J. Singh: *Phys. Rev. B* **78** (2008) 094511.
- 21) F. Ma, Z. Lu, and T. Xiang: arXiv: 0806.3526.
- 22) G. Xu, H. Zhang, X. Dai, and Z. Fang: arXiv:0807.1401.
- 23) H. Q. Yuan, J. Singleton, F.F. Balakirev, S. A. Baily, G. F. Chen, J. L. Luo, and N. L. Wang: *Nature* **457** (2009) 565.

- 24) M. A. Tanatar, N. Ni, C. Martin, R. T. Gordon, H. Kim, V. G. Kogan, G. D. Samolyuk, S. L. Bud'ko, P. C. Canfield, and R. Prozorov: *Phys. Rev. B* **79** (2009) 094507.
- 25) M. Kano, Y. Kohama, D. Graf, F. F. Balakirev, A. S. Sefat, M. A. McGuire, B. C. Sales, D. Mandrus, and S. W. Tozer: arXiv: 0904.1418.
- 26) P. Vilmercati, A. Fedorov, I. Vobornik, Manju U., G. Panaccione, A. Goldoni, A. S. Sefat, M. A. McGuire, B. C. Sales, R. Jin, D. Mandrus, D. J. Singh, and N. Mannella: arXiv:0902.0756.
- 27) C. Liu, T. Kondo, N. Ni, A. D. Palczewski, A. Bostwick, G. D. Samolyuk, R. Khasanov, M. Shi, E. Rotenberg, S. L. Bud'ko, P. C. Canfield, and A. Kaminski: *Phys. Rev. Lett.* **102** (2009) 167004.
- 28) Y. Nakajima, T. Taen, and T. Tamegai: *J. Phys. Soc. Jpn.* **78** (2009) 023702.
- 29) P. Blaha, K. Schwarz, G. K. H. Madsen, D. Kvasnicka, and J. Luitz: *An augmented plane wave + local orbitals program for calculationg crystal properties*, Technische Universitat Wien (2002) Austria; <http://www.wien2k.at>.
- 30) Y. Sekiba, T. Sato, K. Nakayama, K. Terashima, P. Richard, J. H. Bowen, H. Ding, Y.-M. Xu, L. J. Li, G. H. Cao, Z.-A. Xu, and T. Takahashi: *New Journal of Phys.* **11** (2009) 025020.
- 31) D. Hsieh, Y. Xia, L. Wray, D. Qian, K. K. Gomes, A. Yazdani, G. F. Chen, J. L. Luo, N. L. Wang, and M. Z. Hasan: arXiv:0812.2289.
- 32) J. G. Analytis, R. D. McDonald, J.-H. Chu, S. C. Riggs, A. F. Bangura, C. Kucharczyk, M. Johannes, and I. R. Fisher: arXiv: 0902.1172.
- 33) S. Hüfner: *Photoelectron Spectrsoscopy* (1995) Springer.
- 34) R. Yu, K. T. Trinh, A. Moreo, M. Daghofer, J. A. Riera, S. Haas, and E. Dagotto: *Phys. Rev. B* **79** (2009) 104510.
- 35) V. Vildosola, L. Pourovskii, R. Arita, S. Biermann, and A. Georges: *Phys. Rev. B* **78** (2008) 064518.
- 36) M. Rotter, M. Tegel, and D. Johrendt: *Phys. Rev. Lett.* **101** (2008) 107006.

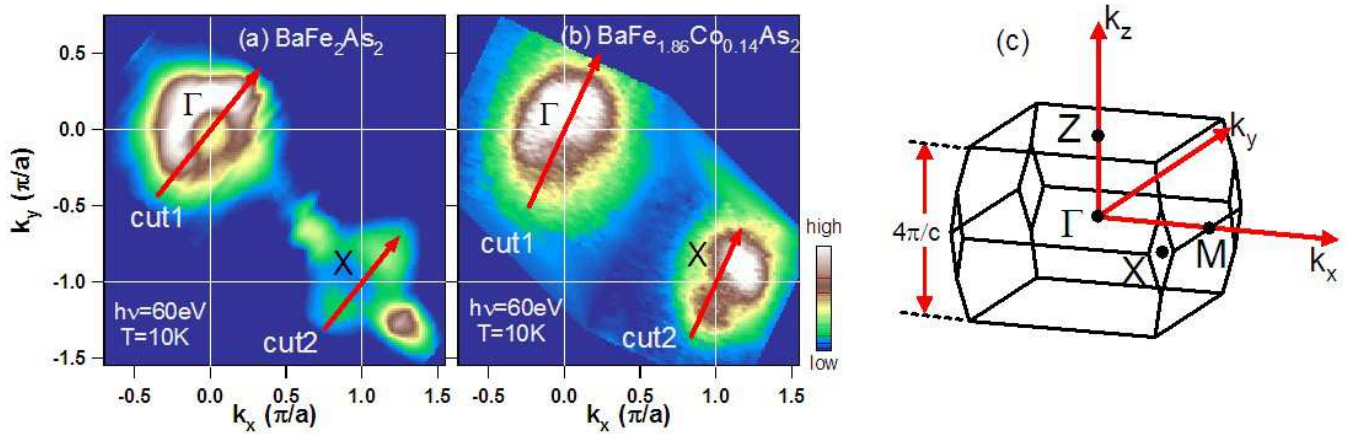


Fig. 1. (Color online) Fermi surface mapping at  $T=10$  K and  $h\nu=60$  eV in the  $k_x$ - $k_y$  plane. The intensity has been integrated within a window of 20 meV around  $E_F$  (a):  $\text{BaFe}_2\text{As}_2$ . (b):  $\text{BaFe}_{1.86}\text{Co}_{0.14}\text{As}_2$ . Red arrows indicate the directions of the cuts for which the results are shown in Figs. 2 and 3. (c): Three-dimensional Brillouin zone of  $\text{BaFe}_{2-x}\text{Co}_x\text{As}_2$  in the tetragonal phase.

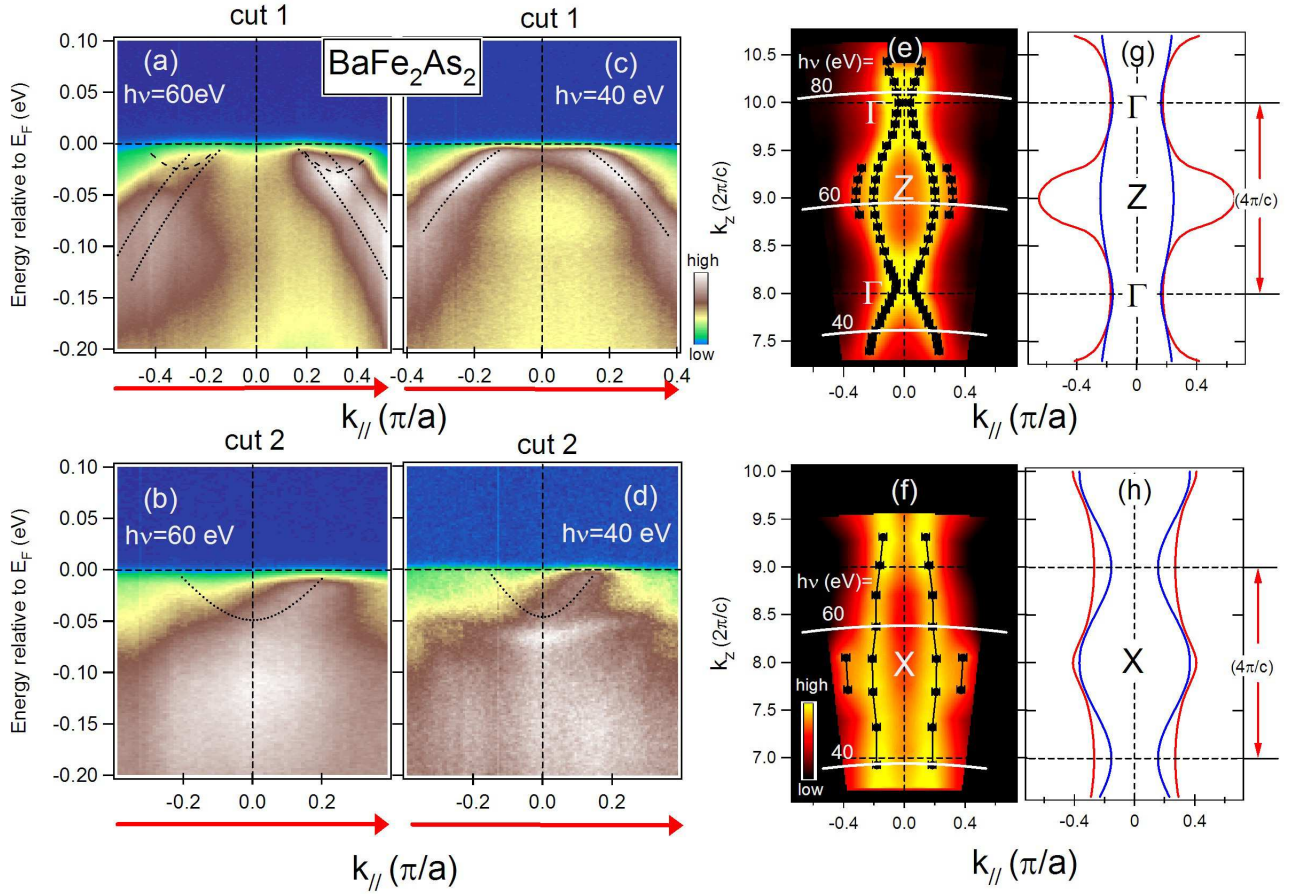


Fig. 2. (Color online) ARPES  $E$ - $k$  intensity maps for  $\text{BaFe}_2\text{As}_2$  taken at  $T=10$  K. (a), (c): Along cut 1 in Fig.1(a). (b), (d): Along cut 2 in Fig. 1 (a). The photon energies are indicated inside each panel. The black curves are guides to the eye. The dashed curves indicate an electron pocket-like feature. (e), (f): Fermi surface images of  $\text{BaFe}_2\text{As}_2$  in the  $k_{||} - k_z$  plane obtained from the  $h\nu$ -dependent ARPES data taken, respectively, along cut 1 and cut 2 in Fig. 1 (a). The photoemission intensities have been integrated in a window of 20 meV around  $E_F$  and finally symmetrized about  $k=0$ . Both inner and outer black dots represent the  $k_F$  values determined from MDC peak positions at  $E_F$ . (g), (h): Fermi surfaces of  $\text{BaFe}_2\text{As}_2$  around the  $\Gamma$  and X points, respectively, determined by LDA band-structure calculations with  $k_{||}$  parallel to the X-Z line and hence approximately to cut 1 and cut 2 in Fig. 1 (a).

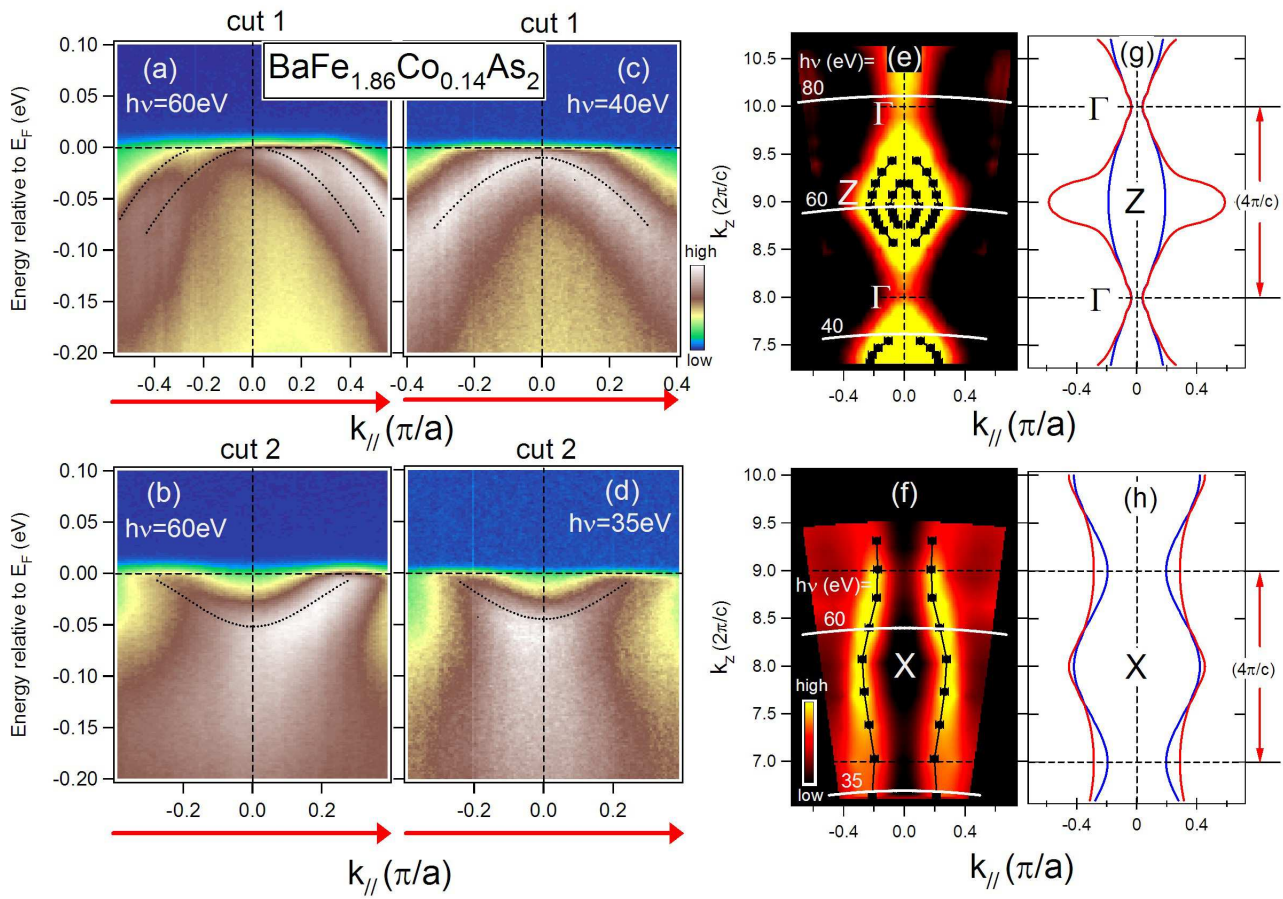


Fig. 3. (Color online) The same as Fig. 2 but for  $\text{BaFe}_{1.86}\text{Co}_{0.14}\text{As}_2$  along cut 1 and cut 2 in Fig. 1 (b).